Author/s:
Thurgood, P;Suarez, SA;Pirogova, E;Jex, AR;Peter, K;Baratchi, S;Khoshmanesh, K

Title:
Tunable Harmonic Flow Patterns in Microfluidic Systems through Simple Tube Oscillation

Date:
2020-10-01

Citation:
Thurgood, P., Suarez, S. A., Pirogova, E., Jex, A. R., Peter, K., Baratchi, S. & Khoshmanesh, K. (2020). Tunable Harmonic Flow Patterns in Microfluidic Systems through Simple Tube Oscillation. Small, 16 (43), https://doi.org/10.1002/smll.202003612.

Persistent Link:
https://hdl.handle.net/11343/276380

DOI: 10.1002/ ((please add manuscript number))

Article type: Full Paper

Tunable harmonic flow patterns in microfluidic systems through simple tube oscillation

Peter Thurgood, Sergio Aguilera Suarez, Elena Pirogova, Aaron R. Jex, Karlheinz Peter, Sara Baratchi [†], Khashayar Khoshmanesh*,[†]*

Dr. P. Thurgood, S. A. Suarez, Prof. E. Pirogova, A/Prof. K. Khoshmanesh

School of Engineering, RMIT University, Melbourne, VIC 3000, Australia

Email: peter.thurgood@rmit.edu.au, khashayar.khoshmanesh@rmit.edu.au

A/Prof. A. R. Jex

Population Health and Immunity Division, The Walter and Eliza Hall Institute of Medical Research, Parkville, Australia and Faculty of Veterinary and Agricultural Sciences, The University of Melbourne, Parkville, VIC 3052, Australia

Prof. K. Peter

Baker Heart and Diabetes Institute, Melbourne, VIC 3004, Australia

Dr. S. Baratchi

School of Health & Biomedical Sciences, RMIT University,
Bundoora, VIC 3083, Australia

† These authors contributed equally

Keywords: microfluidics, inertial, dynamic flow patterns

Generation of tunable harmonic flows at low cost in microfluidic systems is a persistent and significant obstacle to this field, substantially limiting its potential to address major scientific questions and applications. This work introduces a simple and elegant way to overcome this obstacle. Harmonic flow patterns can be generated in microfluidic structures by simply oscillating the inlet tubes. Complex rib and vortex patterns can be dynamically modulated by changing the frequency and magnitude of tube oscillation and the viscosity of liquid. Highly complex rib patterns and synchronous vortices can be generated in serially connected microfluidic chambers. Similar dynamic patterns can be generated using whole or diluted blood samples without damaging the sample. This method offers unique opportunities for studying complex fluids and soft materials, chemical synthesis of various compounds, and mimicking harmonic flows in biological systems using compact, tunable and low-cost devices.

1. Introduction

Microfluidic systems facilitate the manipulation of liquids within miniaturised structures, which not only reduce the volume of samples but also offer unparalleled opportunities for performing complex, multi-step chemical, biochemical and biological reactions under highly controlled conditions.[1, 2] Microfluidic systems are dominated by viscous forces, resulting in highly ordered, laminar flows that mitigate flow disturbances.[3, 4] This improves their control and predictability, but negates many complex tasks that require the ability to generate customised disturbed flows. Generation of disturbed flows enhances the exchange of mass, momentum and heat in microfluidic systems benefiting a variety of applications in physics, chemistry, biology, materials sciences, and bioengineering. This includes studying mechanical and rheological properties of complex fluids and soft materials such as polymers, emulsions, colloids, liquid crystals and their biological counterparts [5-10], chemical synthesis of hazardous chemical compounds, pharmaceutical agents and micro/nanomaterials [11-14], and mimicking harmonic/disturbed flows occurring in the natural systems, such as the human circulatory system, where they may cause dysfunction or disease [15-19].

Passive and active mechanisms have been used to generate disturbed flow patterns in microfluidic systems.[20] The passive mechanisms take advantage of asymmetric geometries or sudden changes in the geometry to generate secondary flows.[21, 22] Examples include patterning asymmetric ridges to induce asymmetric vortices [23], curved channels to generate Dean vortices [24, 25], and sudden expansion of the channel to induce vortices within the expanded regions [26-29]. The vortex characteristics can be modulated by varying the flow rate but largely depend on the configuration of the microfluidic structure, which cannot be changed once fabricated, limiting the versatility, dynamism and compatibility of the system.

In comparison, active mechanisms take advantage of external stimuli to disturb flow. This includes a variety of mechanical [30-32], pneumatic [10, 33-35], thermal [36], acoustic [37, 38], electrical [39, 40], and

electrowetting [41, 42] mechanisms to disturb the laminar flow. Despite these advances, their widespread application has been limited by their dependence on additional supporting equipment, which increases the overall size, cost and complexity of the system, contradicting the principal promises of microfluidics for delivering small, inexpensive and simple devices [43]. In addition, current active methods can damage biological samples [36], limiting their use in biomedical fields. Moreover, these mechanisms are often sensitive to the thermophysical properties of the liquid [40, 41] or specific to the design and geometry of microfluidic structures, limiting their versatility. Tube oscillation is an alternative method for inducing flow instabilities. This method has been used for generating transitional flow patterns in horizontal and vertical tubes [44-48] and has been proven to alter the viscous pressure drop [49] and heat transfer [50] characteristics of tubes. Particularly, it has been shown as an effective method for altering the laminar-turbulent transition in tubes [51-53], which is essential for improving the performance of convective heat exchangers [54]. Despite these advances, tube oscillation has not been applied for the generation of harmonic flow patterns in biologically relevant liquids such as blood within multi-inlet microfluidic structures.

Here, we generate tunable harmonic flow patterns in microfluidic systems by simply oscillating their inlet tubes using standard vortexer mixers. Tube oscillation induces lateral and axial velocities, leading to harmonic changes of the flow velocity profile. This feature is utilised to generate harmonic flows in the form of ribs and vortices in a microfluidic flow focusing system. We show the ability to generate customised harmonic patterns by changing the magnitude and frequency of tube oscillation. We also show the generation of harmonic patterns in water-based solutions at various viscosities as well as blood samples at various dilution ratios. Furthermore, we investigate the generation of complex harmonic patterns in serially connected microfluidic structures. A comprehensive set of experimental, numerical and theoretical analyses is conducted to characterise

the dynamics of these harmonic patterns. The proposed technology only needs standard vortexer mixers that are standard tools in biological laboratories and can be easily interfaced with various multi-inlet microfluidic devices. Notably, this approach overcomes the cost, complexity, fabrication, integration and specificity to the microfluidic design obstacles faced by existing mechanisms and does not appear to impact on the sample integrity. The versatility of this mechanism provides a new and widely accessible method for contact-free manipulation of biological fluids in microfluidic systems.

2. Results and Discussions

2.1. Principles of harmonic flow oscillation

Our experimental setup consisted of a microfluidic flow focusing system (**Figure S1**) coupled with a pair of 5 mL syringes using 40 cm long Tygon® tubes. The syringes were filled with red and blue food dye solutions for flow visualisation. The height of the syringes was set to 10 cm to generate sufficient pressure to drive the coloured solutions though the microfluidic system at 60 µL/min. The tube interfacing the core inlet (carrying red solution) was interfaced with the spindle of a commercially available vortexer (**Figure 1a**). In this manner, the tube could be oscillated at desired frequencies by simply turning the speed control knob of the vortexer. A photo of the experimental setup is shown in **Figure S2**.

The oscillation of the tube induces lateral and axial velocities (**Figure 1b**), which can be expressed as $U_{lateral} = \lambda_{tube}\,\omega_{tube}\sin\omega_{tube}t$ and $U_{axial} = \lambda_{tube}\,\omega_{tube}\cos\omega_{tube}t$, in which λ_{tube} and ω_{tube} are the magnitude and angular frequency of tube oscillation, respectively, and t is time. The

lateral velocity of the tube induces a pressure gradient along the radial axis (**Movie S1** + **Figure S3**). This generates a pair of vortices in the upper and lower halves of the tube, as the liquid moves toward the low-pressure side, bounces back once reaching the tube wall and returns along the tube walls (**Figure 1c**). On the other hand, the axial velocity of the tube imposes a pressure gradient along the longitudinal axis, which pushes the liquid forward and backward (**Movie S1** + **Figure S4**). The combination of dynamic velocities induced by the tube oscillation and the constant velocity induced by gravity leads to the harmonic variation of velocity vectors through the tube (**Figure 1d**) and consequently the liquid flow rate (**Figure 1e**). The motionless portions of the tube and the microfluidic channel act as a viscous damper and reduce the magnitude of velocity oscillation before reaching the flow focusing junction. Given that the inlet pressure of the sheath flow was fixed, the harmonic variations of the core flow rate led to the harmonic expansion and collapse of the core flow within the mixing channel in a cyclic manner, which in turn formed harmonic arrow-shaped flow patterns within the expansion chamber (**Movie S2** + **Figure 1f**).

The frictional losses within the electric motor and rotating shaft of the vortexer led to heating of the vortexer after ~3 min of continuous operation. Measurements using a thermal imaging camera (FLIR C2) indicated a temperature rise of ~1.3°C at the middle of the oscillating tube where it was attached to the vortexer spindle when operating at 40 Hz for 5 min (**Figure S5**). We did not observe any noticeable change in the dynamics of oscillating flow when operating the vortexer continuously for 10 min.

2.2. Generation of the harmonic rib and vortex patterns

First, we characterised the harmonic flow patterns generated by oscillating the tube carrying the core flow at different frequencies as well as liquid viscosities. The magnitude of the core tube oscillation was set to 2.5 mm by attaching the tube to the spindle of a vortexer. The frequency of tube oscillation varied from 14 to 50 Hz. The viscosity of the core flow was adjusted by adding glycerol to the core liquid, allowing us to change the core-to-sheath viscosity ratio ($\varphi = \mu_{core}/\mu_{sheath}$, in which μ_{core} is the core viscosity and μ_{sheath} is the sheath viscosity) from 1 to 5. Numerical simulations reveal that the magnitude of flow rate variations increases linearly with respect to the frequency of tube oscillation (**Figure 2a-b + Figure S6**), which in turn impact the harmonic flow patterns observed in the expansion chamber.

Experiments at $\varphi = 1$ led to the generation of two distinct dynamic flow patterns. This involved the formation of ribs at frequencies ranging from 14 to 23 Hz, which is referred to as 'rib mode', and the formation of vortices at frequencies ranging from 24 to 40 Hz, which is referred to as 'vortex mode' (**Movie S3** + **Figure 2c**). The 'rib mode' was associated with the formation of harmonic ribs along the mixing chamber caused by the transient expansion of the core flow. The 'vortex mode' was associated with the generation of a pair of vortices at the inlet of the expansion chamber, which are referred to as *leading vortices*. The change of core flow direction (due to the induction of axial tube velocity) led to contraction of the leading vortices, resulting in the generation of a pair of vortices at the outlet of the expansion chamber, which are referred to as *trailing vortices* (**Figure S7**). The leading and trailing vortices were generated and degenerated in a competitive manner. The trailing vortices were smaller than the leading vortices due to the incorporation of the static component of the core flow velocity, $U_{core} = U_o + U_{axial}$. Increase of oscillation frequency resulted in the gradual expansion of the vortices until they occupied the entire expansion chamber. Harmonic ribs were formed in the vortex-free region of the expansion chamber.

Similar dynamic flow patterns were observed when increasing the viscosity ratio to $\varphi = 2$ (**Movie S3** + **Figure 2d**) and $\varphi = 5$ (**Movie S3** + **Figure 2e**). However, the increased core viscosity was associated with an increased number of ribs, as the core flow moved slower and therefore could be oscillated more often. The core viscosity also changed the configuration of the ribs with respect to the core flow, resulting in the formation of backward, straight and forward swept ribs at $\varphi = 1$, 2 and 5, respectively. In fact, the configuration of the ribs is determined by the velocity profile of the flow across the width of the expansion chamber. Numerical simulations revealed the consistent reduction of the core flow velocity in response to increased core viscosity, resulting in the ratio between the peak flow velocities at the middle and sides of the expansion chamber, defined as $\xi = U_{middle-max}/U_{sides-max}$, to reduce from ~1 at $\varphi = 1$ to 0.56 at $\varphi = 2$ and 0.25 at $\varphi = 5$ (**Figure S8**), causing the ribs to sweep backward, straight and forward, respectively. The increased core viscosity also reduced the extent of the vortices within the expansion chamber due to the dominance of viscous effects.

In order to describe the dynamic characteristics of the system, we defined the Reynolds number of the oscillating core flow as $Re_{core} = \rho_{core}\ \bar{U}_{core}\ D_{tube}/\mu_{core}$, in which ρ_{core} and μ_{core} are the density and viscosity of the core flow, respectively, D_{tube} is the internal diameter of the oscillating tube, and $\bar{U}_{core}$ is the equivalent velocity of the core flow induced by tube oscillation. $\bar{U}_{core}$ was obtained by balancing the dynamic pressure caused by tube oscillation with the viscous pressure drop along the tube and the corresponding microfluidic channel:

$$\Delta P_{oscillation} = \Delta P_{viscous-tube} + \Delta P_{viscous-channel} \quad (1)$$

The dynamic pressure caused by tube oscillation is defined as:

$$\Delta P_{oscillation} = 0.5\ \rho_{core}\,(\lambda_{tube}\ \omega_{tube})^2 \quad (2)$$

Accordingly, the viscous pressure drop along the tube and channel are defined as:

$$\Delta P_{viscous-tube} = 128\,\mu_{core}\,Q_{core}\,L_{tube}/\pi D_{tube}^{2} \qquad (3)$$

$$\Delta P_{viscous-channel} = a\,\mu_{core}\,Q_{core}\,L_{ch}/W_{ch}H_{ch}^{3} \qquad (4)$$

in which $Q_{core} = \bar{U}_{core}\,\pi D_{tube}^{2}/4$ is the equivalent dynamic flow rate of oscillating core flow, L_{tube} is the length of the oscillating tube, L_{ch}, W_{ch} and H_{ch} are the length, width and height of the microfluidic channel lying between the core inlet and the junction of flow focusing system, and $a = 12[1-(192\,H_{ch}/\pi^{5}W_{ch})\tanh(\pi\,W_{ch}/2\,H_{ch})]^{-1}$ is the theoretical aspect ratio coefficient [55], based on which, Q_{core} is obtained based on the magnitude and frequency of tube oscillation, properties of the core liquid, as well as dimenstsions of the oscillating tube and the microfluidic channel:

$$\bar{Q}_{core} \propto \underbrace{\lambda_{tube}^{2}, \omega_{tube}^{2}}_{\text{oscillation}}, \underbrace{\rho_{core}, \mu_{core}^{-1}}_{\text{core flow}}, \underbrace{L_{tube}^{-1}, D_{tube}^{4}}_{\text{tube}}, \underbrace{L_{ch}^{-1}, W_{ch}, H_{ch}^{3}}_{\text{channel}} \qquad (5)$$

The core and sheath flows come across each other at the proximity of the junction (**Figure 1e**). The diffusive mixing occurring at the interface of the core and sheath flows reduces the viscosity contrast between the flows. This suggests a reduction in the viscosity of the core flow, and consequently the viscous pressure drop inside the microfluidic channel ($\Delta P_{viscous-channel}$) when $\varphi > 1$. To take this effect into account, we multiplied the Reynolds number of oscillating core flow by a dilution factor, and defined the equivalent Reynolds number of adjacent core and sheath flows as $Re_{core-sheath} = Re_{core}\,\varphi^{1.5}$. The inclusion of $\varphi^{1.5}$ was essential to predict the generation of instability patterns when $\varphi > 1$.

Using the Reynolds number of the oscillating tube, we described the dynamics of the core flow using a polar map (**Figure 2f**), in which the location of the points along the radial axis is determined by

$Re_{core-sheath}$ while the polar angle of the points is determined by φ. The transition from 'rib' to 'vortex' mode occurred at $0.32 \leq Re_{core-sheath} \leq 0.4$. Further analysis indicated that the extension of the *leading* and *trailing* vortices inside the expansion chamber changes linearly with respect to the Reynolds number $L_{vortex}/L_{chamber} \propto Re_{core-sheath}$ (**Figure S9**). To further explore the versatility of the proposed mechanism, we studied the generation of harmonic flows under various operating conditions, as discussed below:

Syringe pump: Our experiments indicated the ability to generate harmonic rib and vortex patterns when driving the core and sheath flows through the microfluidic system using a syringe pump (**Movie S4 + Figure S10**).

Tube diameter: Increasing the internal diameter of the oscillating tube from 500 to 800 µm, reduced the viscous pressure drop along the tube (a 17% increase in $Re_{core-sheath}$) and increased the tendency of the core flow for the generation of harmonic rib and vortex patterns (**Movie S5 + Figure S11**).

Tube length: Increasing the length of both core and sheath tubes from 40 to 80 cm, doubled the viscous pressure drop along the tube (a 35% decrease in $Re_{core-sheath}$) and limited the ability of the tube oscillation mechanism to generate harmonic flows (**Movie S6 + Figure S12**). Nevertheless, doubling the tube length enables the vortexer to be kept away from the microscope.

Geometry of the expansion chamber: Decreasing the cross-sectional dimensions of the microfluidic channel from 160 µm × 160 µm to 80 µm × 80 µm, increased the viscous pressure drop along the channel by a factor of 16 (an 87% decrease in $Re_{core-sheath}$) and impaired the ability of the tube oscillation mechanism to generate vortex patterns inside the expansion chamber. In contrast, doubling the width or halving the length of the expansion chamber did not change the dynamic

characteristics of harmonic flow patterns and only changed the size of the harmonic rib or vortex patterns (**Movie S7 + Figure S13**).

Location of the vortexer: Our experiments indicated that the location of the vortexer along the oscillating tube does not have any noticeable effect on the dynamics of the harmonic flow patterns (**Movie S8 + Figure S14**). Similar harmonic patterns were obtained when relocating the vortexer by ±5 cm with respect to the middle of the oscillating tube.

Next, we characterised the instability flow patterns when reducing the magnitude of the core tube oscillation to 0.5 mm. This was achieved by attaching the tube to the sidewall of the vortexer. Experiments were conducted at tube oscillation frequencies ranging from 14 to 50 Hz and viscosity ratios of $\varphi = 1$, 2 and 5. Numerical simulations reveal that the magnitude of flow rate variations increases linearly with respect to the frequency of tube oscillation, similar to that obtained at high magnitude oscillations (**Figure 3a-b + Figure S6**).

Our experiments indicated the dominance of 'rib mode' characterised by the generation of harmonic rib patterns across the entire range of frequencies and viscosity ratios (**Movie S9** + **Figure 3c-e**). Increasing the frequency of tube oscillation or the viscosity ratio led to increasing the number of ribs, in line with our observations in the in Fig. 2 (**Figure S15**). Increasing the viscosity ratio ($\varphi \geq 2$) caused the ribs to sweep forward due to the velocity contrast between the core and sheath flows (**Figure S16**). Our further analysis indicated that the Reynolds number of the expansion chamber was limited to 0.066 (**Figure 3f**). This was much smaller than the transitional range of $0.32 \leq Re_{core-sheath} \leq 0.4$, beyond which harmonic vortices would be generated, justifying the dominance of the 'rib mode' in the expansion chamber.

2.3. Dynamic flow patterns in blood

Next, we studied the generation of dynamic flow patterns of human blood in the microfluidic system. In the first set of experiments, blood was applied as the core flow while Hanks' balanced salt solution (HBSS) buffer was applied as the sheath flow (**Figure 4a**). Experiments were performed using whole blood as well as blood samples diluted with HBSS at 1:10 and 1:25 volumetric ratios. The core tube was oscillated at both low and high magnitudes of 0.5 and 2.5 mm and frequencies ranging from 14 to 50 Hz.

Our experiments indicated the formation of dynamic flow patterns in blood were similar to water-based solutions (**Figures 2 and 3**). This involved the formation of 'ribs' and 'vortices' when setting the magnitude of tube oscillation magnitude to 2.5 mm, and the formation of only 'ribs' when reducing the magnitude of tube oscillation to 0.5 mm (**Movie S10** + **Figure 4b-d**). Notably, the destabilisation of the core flow was associated with the dispersion of blood cells within the chamber.

The flow pattern map of oscillating blood sheathed by HBSS, is presented in **Figure 4e**. The location of the points along the radial axis is determined by their Reynolds number, which is defined as $Re_{blood-HBSS} = Re_{blood}\ \varphi^{1.5}$, and the polar angle of the points is determined by the dilution ratio of the blood samples. The transition from 'rib' to 'vortex' mode occurred when $0.32 \leq Re_{core-sheath} \leq 0.4$, which is in line with the results obtained for water-based solutions.

In the second set of experiments, the blood and HBSS were swapped such that the blood was applied as the sheath flow and the HBSS was applied as the core flow (**Figure 4f**). Our experiments indicated the formation of oscillating 'ribs' and 'vortices' (**Movie S11** + **Figure 4g-i**). The flow pattern map of oscillating HBSS sheathed by blood, is presented in **Figure 4j**. The location of the points along

the radial axis was determined by the Reynolds number of oscillating HBSS, defined as $Re_{HBSS-blood} = Re_{HBSS}$. In this case, the core flow had a lower viscosity compared to the sheath flow ($\varphi \leq 1$), and the viscosity ratio correction factor ($\varphi^{1.5}$) was not included in the calculation of $Re_{HBSS-blood}$. The transition from 'rib' to 'vortex' mode occurs when $0.32 \leq Re_{core-sheath} \leq 0.4$, which in in line with the results obtained for the case of oscillating blood.

To assess the potential impact of our method on the integrity of the blood samples, we tested for haemolysis of red blood cells by measuring the haemoglobin level in free plasma before and after high-magnitude tube oscillation at 14, 25 and 40 Hz. Based on our measurements, the highest percentage of haemolysis obtained at 40 Hz was ~5%, confirming the biocompatibility of the tube oscillation mechanism (**Figure S17**). Compared to existing disturbed flow methods, the tube oscillation mechanism minimises cell damage caused by contact with the sharp, moving edges of mechanical pumps [31], minimises fouling and cross-contamination due to contact with elastomeric membranes of pneumatic or piezoelectric pumps [56, 57], is not sensitive to physio-chemical properties of blood [40, 41], and does not expose blood samples to thermal, optical, chemical and electrical stimuli [36, 41].

2.4. Generation of complex harmonic flows in serial microfluidic chambers

We also studied the generation of complex dynamic flow patterns using two serially connected expansion chambers. The length of the chambers was reduced to 45% to facilitate the microscopic observation of both chambers with a small interconnecting gap. Experiments were conducted using water-glycerol against water at viscosity ratios of φ=1 and 3 as well as blood samples diluted at

volumetric ratios of 1:10 and 1:25 against HBSS. The core tube was oscillated at both low and high magnitudes of 0.5 and 2.5 mm and frequencies within the range of 14 to 50 Hz.

Our experiments indicated the superposition of harmonic ribs in the second expansion chamber (**Movie S12** + **Figure 5a-b**). The ribs generated in the first chamber were squeezed while passing through the narrow channel connecting the two chambers. This enabled the ribs to be carried to the second chamber without being decayed. The oscillation of the core flow led to the formation of secondary ribs in the second chamber, which superimposed onto the initial ribs. This resulted in complex dynamic flow patterns to be generated in the second chamber while maintaining the same number of ribs. For the case of vortices, the oscillation of the core flow led to the generation of synchronous vortices in both chambers (**Movie S12** + **Figure 5c-e**). This significantly enhanced the mixing of the core and sheath flows in the second chamber. The flow pattern map of oscillating core flow is presented in **Figure 5f**.

3. Conclusion

In summary, we demonstrated the generation of harmonic flow patterns in microfluidics by simply oscillating the inlet tubes of the device using a commercially available vortexer commonly used in biological labs. We demonstrated the formation of harmonic ribs and vortices in a microfluidic flow focusing system. We also characterised the dynamics of flow against various tube oscillation frequencies and magnitudes as well as liquid viscosities, based on which we provided the flow pattern map of the system. We demonstrated the generation of complex rib patterns and

synchronous vortices in serially connected microfluidic chambers. Importantly, we were also able to generate harmonic flow patterns in both whole and diluted blood samples.

The simplicity, controllability, versatility and biocompatibility of the newly described technology makes it highly suitable for multiple applications. These include important applications in physics (e.g. studying complex fluids and soft materials [5-7], and generation of droplets [58, 59]), chemistry (e.g. synthesis of various molecules and compounds [11, 12]), and biology (e.g. manipulation of cells [60, 61], performing multi-step assays [13], diagnostics [62], and developing organ-on-a-chip platforms [63] for studying the mechanobiology of cells [64, 65] and the human circulatory system [17, 19, 66]). Notably, both customised harmonic and disturbed flow patterns can be created and studied using the newly described technology.

4. Experimental Section

Microfluidic structures: SU-8 masters were fabricated by spin coating SU-8 3050 photoresist (Microchem) onto 4-inch silicon wafers and patterned using a maskless aligner (MLA150, Heidelberg Instruments). PDMS (Sylgard 184, Dowsil) was mixed to a ratio of 10:1 w/w and degassed under vacuum prior to pouring onto the SU-8 master. The PDMS was then cured at 120°C for 25 minutes and peeled off the master. The PDMS slabs were then cut to size with a scalpel and liquid interfaces were cut using a biopsy punch (Harris uni-core). The slabs were then permanently bonded to a glass sides (75 mm × 25 mm × 1 mm, Thermo Scientific) following plasma treatment (PDC-002, Harrick Plasma). Microfluidic structure designs are shown in **Figure S1**.

Imaging: The microfluidic experiments were monitored using an upright microscope (Leica DM2500) coupled with a colour CMOS camera (acA1920-155uc, Basler, Germany) recording at ~150 frames per second. The images were analysed and measured using ImageJ.

Experimental setup: The experimental setup consisted of a pair of 5 mL liquid filled syringes (Braun) coupled to a PDMS based microfluidic chip using Tygon® tubes (ID = 0.5 mm, OD = 1.5 mm, L = 40 cm). The syringes were kept 10 cm above the microfluidic system to act as gravity-based pumps. In order to induce lateral oscillations, the inlet tube (core or sheath) was coupled to a vortexer mixer (SBS100, Select BioProducts) in two operating modes, including the the *high-magnitude oscillation* mode, in which the tube was directly coupled to the vortexer spindle and the *low-magnitude oscillation*, in which the tube was coupled to the side of the vortexer chassis with clear adhesive tape.

Numerical simulations: Computational fluid dynamics simulations were conducted to analyse the flow velocity induced by tube oscillation. Simulations were performed using ANSYS Fluent 6.3 software (ANSYS Inc., Canonsburg, PA). To do so, Navier-Stokes differential equations governing the balance of mass and momentum were solved in three dimensions and transient conditions under laminar flow regime. The SIMPLEC (Semi-Implicit Method for Pressure Linked Equations-Consistent) algorithm was utilised for coupling of pressure-velocity terms while second-order upwind scheme was utilised for discretization of convective terms [67]. The boundary conditions included a fixed pressure at the inlet, zero pressure at the outlet, no-slip, zero velocity conditions across the motionless sections of the tube while harmonic velocities along the radial and axial axes of the tube

across the oscillating sections of the tube, defined as $U_{lateral} = \lambda_{tube}\,\omega_{tube}\sin\omega_{tube}t$ and $U_{axial} = \lambda_{tube}\,\omega_{tube}\cos\omega_{tube}t$, in which λ_{tube} and ω_{tube} are the magnitude and angular frequency of tube oscillation, respectively, and t is time.

Human blood preparation: Fresh peripheral blood samples were acquired from healthy individuals and collected in 10 mL S-Monovettes (Sarstedt, Germany) containing 3.2% buffered sodium citrate to be used within five hours of blood sampling. Both whole and diluted blood samples were used in our experiments. Blood samples were diluted with calcium/magnesium free Hanks' balanced salt solution (HBSS) containing 2 mM ethylenediaminetetraacetic acid (EDTA) to prevent coagulation. The study was approved by the Alfred Ethics Committee. The haemolysis was assessed by measuring the absorbance of haemoglobin at 414 nm using a NanoDrop™ 1000 spectrophotometer (Thermo Scientific, Australia) in free plasma before and after high-magnitude tube oscillation experiments. The positive control was obtained by diluting the red blood cells in DI water and vigorous pipetting to lyse the cells.

Supporting Information

Supporting Information is available from the Wiley Online Library or from the author.

Acknowledgements

The authors wish to acknowledge RMIT's MicroNano Research Facility (MNRF) for the fabrication of microfluidic devices. A. R. J. acknowledges the Australian National Health and Medical Research Foundation Career Development Fellowship program (APP1126395). A. R. J. also acknowledges funding from the Victorian State Government Operational Infrastructure Support and Australian

Government National Health and Medical Research Council (NHMRC) Independent Research Institute Infrastructure Support Scheme. E. P. acknowledges NHMRC for funding 'The Australian Centre for Electromagnetic Bioeffects Research' (NHMRC CRE APP1135076). K. P. acknowledges the NHMRC for the Principal Research Fellowship (GNT1079492). S. B. acknowledges the Australian Research Council (ARC) for Discovery for Discovery Grant (DE170100239 and DP200101248). A. R. J. and K. K. acknowledge ARC for Discovery Grant (DP180102049).

Received: ((will be filled in by the editorial staff))
Revised: ((will be filled in by the editorial staff))
Published online: ((will be filled in by the editorial staff))

References

[1] Whitesides, G. M., *Nature* **2006,** *442* (7101), 368-373. DOI 10.1038/nature05058.

[2] Yang, Y.; Chen, Y.; Tang, H.; Zong, N.; Jiang, X., *Small Methods* **2020,** *4* (4). DOI 10.1002/smtd.201900451.

[3] Stone, H. A.; Kim, S., *AIChE J* **2001,** *47* (6), 1250-1254. DOI 10.1002/aic.690470602.

[4] Squires, T. M.; Quake, S. R., *Rev Mod Phys* **2005,** *77* (3), 977-1026. DOI 10.1103/RevModPhys.77.977.

[5] Granick, S.; Zhu, Y.; Lee, H., *Nat Mater* **2003,** *2* (4), 221-227. DOI 10.1038/nmat854.

[6] Mitov, M., *Soft Matter* **2017,** *13* (23), 4176-4209. DOI 10.1039/C7SM00384F.

[7] Keshavarz, B.; Houze, E. C.; Moore, J. R.; Koerner, M. R.; McKinley, G. H., *Phys Rev Fluids* **2020,** *5* (3), 033601. DOI 10.1103/PhysRevFluids.5.033601.

[8] Bian, F.; Sun, L.; Cai, L.; Wang, Y.; Wang, Y.; Zhao, Y., *Small* **2020,** *16* (9). DOI 10.1002/smll.201903931.

[9] Hopkins, C. C.; Haward, S. J.; Shen, A. Q., *Small* **2020,** *16* (9). DOI 10.1002/smll.201903872.

[10] Asghari, M.; Cao, X.; Mateescu, B.; van Leeuwen, D.; Aslan, M. K.; Stavrakis, S.; deMello, A. J., *ACS Nano* **2020,** *14* (1), 422-433. DOI 10.1021/acsnano.9b06123.

[11] Elvira, K. S.; i Solvas, X. C.; Wootton, R. C. R.; deMello, A. J., *Nat Chem* **2013,** *5* (11), 905-915. DOI 10.1038/nchem.1753.

[12] Liu, Y.; Jiang, X., *Lab Chip* **2017,** *17* (23), 3960-3978. DOI 10.1039/C7LC00627F.

[13] Eduati, F.; Utharala, R.; Madhavan, D.; Neumann, U. P.; Longerich, T.; Cramer, T.; Saez-Rodriguez, J.; Merten, C. A., *Nat Commun* **2018,** *9* (1), 2434. DOI 10.1038/s41467-018-04919-w.

[14] Liu, Z.; Fontana, F.; Python, A.; Hirvonen, J. T.; Santos, H. A., *Small* **2020,** *16* (9). DOI 10.1002/smll.201904673.

[15] Hahn, C.; Schwartz, M. A., *Nat Rev Mol Cell Biol* **2009,** *10* (1), 53-62. DOI 10.1038/nrm2596.

[16] Chiu, J.-J.; Chien, S., *Physiol Rev* **2011,** *91* (1), 327-387. DOI 10.1152/physrev.00047.2009.

[17] Baratchi, S.; Khoshmanesh, K.; Woodman, O. L.; Potocnik, S.; Peter, K.; McIntyre, P., *Trends Mol Med* **2017,** *23* (9), 850-868. DOI https://doi.org/10.1016/j.molmed.2017.07.007.

[18] Dincau, B.; Dressaire, E.; Sauret, A., *Small* **2020,** *16* (9). DOI 10.1002/smll.201904032.

[19] Baratchi, S.; Zaldivia, M. T. K.; Wallert, M.; Loseff-Silver, J.; Al-Aryahi, S.; Zamani, J.; Thurgood, P.; Salim, A.; Htun, N. M.; Stub, D.; Vahidi, P.; Duffy, S. J.; Walton, A.; Nguyen, T. H.; Jaworowski, A.; Khoshmanesh, K.; Peter, K., *Circulation 0* (0). DOI doi:10.1161/CIRCULATIONAHA.120.045536.

[20] Ahmed, H.; Ramesan, S.; Lee, L.; Rezk, A. R.; Yeo, L. Y., *Small* **2020,** *16* (9). DOI 10.1002/smll.201903605.

[21] Amini, H.; Lee, W.; Di Carlo, D., *Lab Chip* **2014,** *14* (15), 2739-2761. DOI 10.1039/C4LC00128A.

[22] Zhang, J.; Yan, S.; Yuan, D.; Alici, G.; Nguyen, N.-T.; Ebrahimi Warkiani, M.; Li, W., *Lab Chip* **2016,** *16* (1), 10-34. DOI 10.1039/C5LC01159K.

[23] Stroock, A. D.; Dertinger, S. K. W.; Ajdari, A.; Mezić, I.; Stone, H. A.; Whitesides, G. M., *Science* **2002,** *295* (5555), 647-651. DOI 10.1126/science.1066238.

[24] Sudarsan, A. P.; Ugaz, V. M., *Proc Natl Acad Sci USA* **2006,** *103* (19), 7228-7233. DOI 10.1073/pnas.0507976103.

[25] Warkiani, M. E.; Tay, A. K. P.; Guan, G.; Han, J., *Sci Rep* **2015,** *5* (1), 11018. DOI 10.1038/srep11018.

[26] Mach, A. J.; Kim, J. H.; Arshi, A.; Hur, S. C.; Di Carlo, D., *Lab Chip* **2011,** *11* (17), 2827-2834. DOI 10.1039/C1LC20330D.

[27] Sollier, E.; Go, D. E.; Che, J.; Gossett, D. R.; O'Byrne, S.; Weaver, W. M.; Kummer, N.; Rettig, M.; Goldman, J.; Nickols, N.; McCloskey, S.; Kulkarni, R. P.; Di Carlo, D., *Lab Chip* **2014,** *14* (1), 63-77. DOI 10.1039/C3LC50689D.

[28] Thurgood, P.; Suarez, S. A.; Chen, S.; Gilliam, C.; Pirogova, E.; Jex, A. R.; Baratchi, S.; Khoshmanesh, K., *Lab Chip* **2019,** *19* (17), 2885-2896. DOI 10.1039/C9LC00618D.

[29] Nguyen, N.; Thurgood, P.; Arash, A.; Pirogova, E.; Baratchi, S.; Khoshmanesh, K., *Adv Func Mater* **2019,** *29* (27), 1901998. DOI 10.1002/adfm.201901998.

[30] Agarwal, A. K.; Sridharamurthy, S. S.; Beebe, D. J.; Hongrui, J., *J Microelectromech Syst* **2005,** *14* (6), 1409-1421. DOI 10.1109/JMEMS.2005.859101.

[31] Ryu, K. S.; Shaikh, K.; Goluch, E.; Fan, Z.; Liu, C., *Lab Chip* **2004,** *4* (6), 608-613. DOI 10.1039/B403305A.

[32] Vedel, S.; Olesen, L. H.; Bruus, H., *J Micromech Microeng* **2010,** *20* (3), 035026. DOI 10.1088/0960-1317/20/3/035026.

[33] Zhou, X.; Zhou, X.; Zheng, B., *Biomicrofluidics* **2013,** *7* (5), 054116. DOI 10.1063/1.4826158.

[34] Khoshmanesh, K.; Almansouri, A.; Albloushi, H.; Yi, P.; Soffe, R.; Kalantar-zadeh, K., *Sci Rep* **2015,** *5* (1), 9942. DOI 10.1038/srep09942.

[35] Kim, S.-J.; Yokokawa, R.; Takayama, S., *Lab Chip* **2013,** *13* (8), 1644-1648. DOI 10.1039/C3LC41415A.

[36] Xu, R.; Xin, H.; Li, B., *AIP Adv* **2013,** *3* (5), 052120. DOI 10.1063/1.4805080.

[37] Chen, C.; Zhang, S. P.; Mao, Z.; Nama, N.; Gu, Y.; Huang, P.-H.; Jing, Y.; Guo, X.; Costanzo, F.; Huang, T. J., *Lab Chip* **2018,** *18* (23), 3645-3654. DOI 10.1039/C8LC00589C.

[38] Collins, D. J.; Khoo, B. L.; Ma, Z.; Winkler, A.; Weser, R.; Schmidt, H.; Han, J.; Ai, Y., *Lab Chip* **2017,** *17* (10), 1769-1777. DOI 10.1039/C7LC00215G.

[39] Bazant, M. Z., Nonlinear Electrokinetic Phenomena. In *Encyclopedia of Microfluidics and Nanofluidics*, Li, D., Ed. Springer New York: New York, NY, 2015; pp 2416-2426.

[40] Chang, S. T.; Beaumont, E.; Petsev, D. N.; Velev, O. D., *Lab Chip* **2008,** *8* (1), 117-124. DOI 10.1039/B712108C.

[41] Tang, S.-Y.; Khoshmanesh, K.; Sivan, V.; Petersen, P.; O'Mullane, A. P.; Abbott, D.; Mitchell, A.; Kalantar-zadeh, K., *Proc Natl Acad Sci USA* **2014,** *111* (9), 3304-3309. DOI 10.1073/pnas.1319878111.

[42] Tang, S.-Y.; Sivan, V.; Petersen, P.; Zhang, W.; Morrison, P. D.; Kalantar-zadeh, K.; Mitchell, A.; Khoshmanesh, K., *Adv Func Mater* **2014,** *24* (37), 5851-5858. DOI 10.1002/adfm.201400689.

[43] Boyd-Moss, M.; Baratchi, S.; Di Venere, M.; Khoshmanesh, K., *Lab Chip* **2016,** *16* (17), 3177-3192. DOI 10.1039/C6LC00712K.

[44] Harris, J.; Peev, G.; Wilkinson, W. L., *J Phys E Sci Instrum* **1969,** *2* (11), 913-916. DOI 10.1088/0022-3735/2/11/301.

[45] Sergeev, S. I., *Fluid Dynamics* **1966,** *1* (1), 121-122. DOI 10.1007/BF01016289.

[46] Teufel, M.; Trimis, D.; Lohmüller, A.; Takeda, Y.; Durst, F., *Flow Meas Instrum* **1992,** *3* (2), 95-101. DOI https://doi.org/10.1016/0955-5986(92)90006-Q.

[47] Amaratunga, M.; Rabenjafimanantsoa, H. A.; Time, R. W., *Flow Meas Instrum* **2019,** *70*, 101628. DOI https://doi.org/10.1016/j.flowmeasinst.2019.101628.

[48] Whittaker, R. J.; Heil, M.; Waters, S. L., *Philos Trans R Soc A* **2011,** *369* (1947), 2989-3006. DOI doi:10.1098/rsta.2011.0106.

[49] Zhuang, N.; Tan, S.; Yuan, H., *Exp Therm Fluid Sci* **2016,** *76*, 352-364. DOI https://doi.org/10.1016/j.expthermflusci.2016.03.030.

[50] Su, Y.; Davidson, J. H.; Kulacki, F., *World Acad Sci Eng Technol* **2011,** *81*, 653-662.

[51] Ohmi, M.; Iguchi, M.; Kakehashi, K.; Masuda, T., *Bull JSME* **1982,** *25* (201), 365-371. DOI 10.1299/jsme1958.25.365.

[52] Ahn, K. H.; Ibrahim, M. B., *Int J Heat Fluid Flow* **1992,** *13* (4), 340-346. DOI https://doi.org/10.1016/0142-727X(92)90004-S.

[53] Trip, R.; Kuik, D. J.; Westerweel, J.; Poelma, C., *Phys Fluids* **2012,** *24* (1), 014103. DOI 10.1063/1.3673611.

[54] Incropera, F. P., DeWitt, D. P., *Fundamentals of heat and mass transfer*. John Wiley & Sons: New York:, **2002**.

[55] Fuerstman, M. J.; Lai, A.; Thurlow, M. E.; Shevkoplyas, S. S.; Stone, H. A.; Whitesides, G. M., *Lab Chip* **2007,** *7* (11), 1479-1489. DOI 10.1039/B706549C.

[56] Mohammed, M.; Thurgood, P.; Gilliam, C.; Nguyen, N.; Pirogova, E.; Peter, K.; Khoshmanesh, K.; Baratchi, S., *Anal Chem* **2019,** *91* (18), 12077-12084. DOI 10.1021/acs.analchem.9b03247.

[57] Lee, Y.-S.; Bhattacharjee, N.; Folch, A., *Lab Chip* **2018,** *18* (8), 1207-1214. DOI 10.1039/C8LC00001H.

[58] Cybulski, O.; Garstecki, P.; Grzybowski, B. A., *Nat Phys* **2019,** *15* (7), 706-713. DOI 10.1038/s41567-019-0486-8.

[59] Heuberger, M.; Gottardo, L.; Dressler, M.; Hufenus, R., *Microfluid Nanofluid* **2015,** *19* (3), 653-663. DOI 10.1007/s10404-015-1592-2.

[60] Lee, J.; Burns, M. A., *Small* **2018,** *14* (9). DOI 10.1002/smll.201702724.

[61] Ciftlik, A. T.; Ettori, M.; Gijs, M. A. M., *Small* **2013,** *9* (16), 2764-2773. DOI 10.1002/smll.201201770.

[62] Nayak, S.; Blumenfeld, N. R.; Laksanasopin, T.; Sia, S. K., *Anal Chem* **2017,** *89* (1), 102-123. DOI 10.1021/acs.analchem.6b04630.

[63] Ingber, D. E., *Development* **2018,** *145* (16). DOI 10.1242/dev.156125.

[64] Deng, Y.; Davis, S. P.; Yang, F.; Paulsen, K. S.; Kumar, M.; Sinnott DeVaux, R.; Wang, X.; Conklin, D. S.; Oberai, A.; Herschkowitz, J. I.; Chung, A. J., *Small* **2017,** *13* (28). DOI 10.1002/smll.201700705.

[65] Liu, A.; Yu, T.; Young, K.; Stone, N.; Hanasoge, S.; Kirby, T. J.; Varadarajan, V.; Colonna, N.; Liu, J.; Raj, A.; Lammerding, J.; Alexeev, A.; Sulchek, T., *Small* **2020,** *16* (2). DOI 10.1002/smll.201903857.

[66] Tovar-Lopez, F.; Thurgood, P.; Gilliam, C.; Nguyen, N.; Pirogova, E.; Khoshmanesh, K.; Baratchi, S., *Front Bioeng Biotechnol* **2019,** *7* (81). DOI 10.3389/fbioe.2019.00081.

[67] J., B., *Computational fluid dynamics: Principles and applications*. Elsevier Science: **2005**.

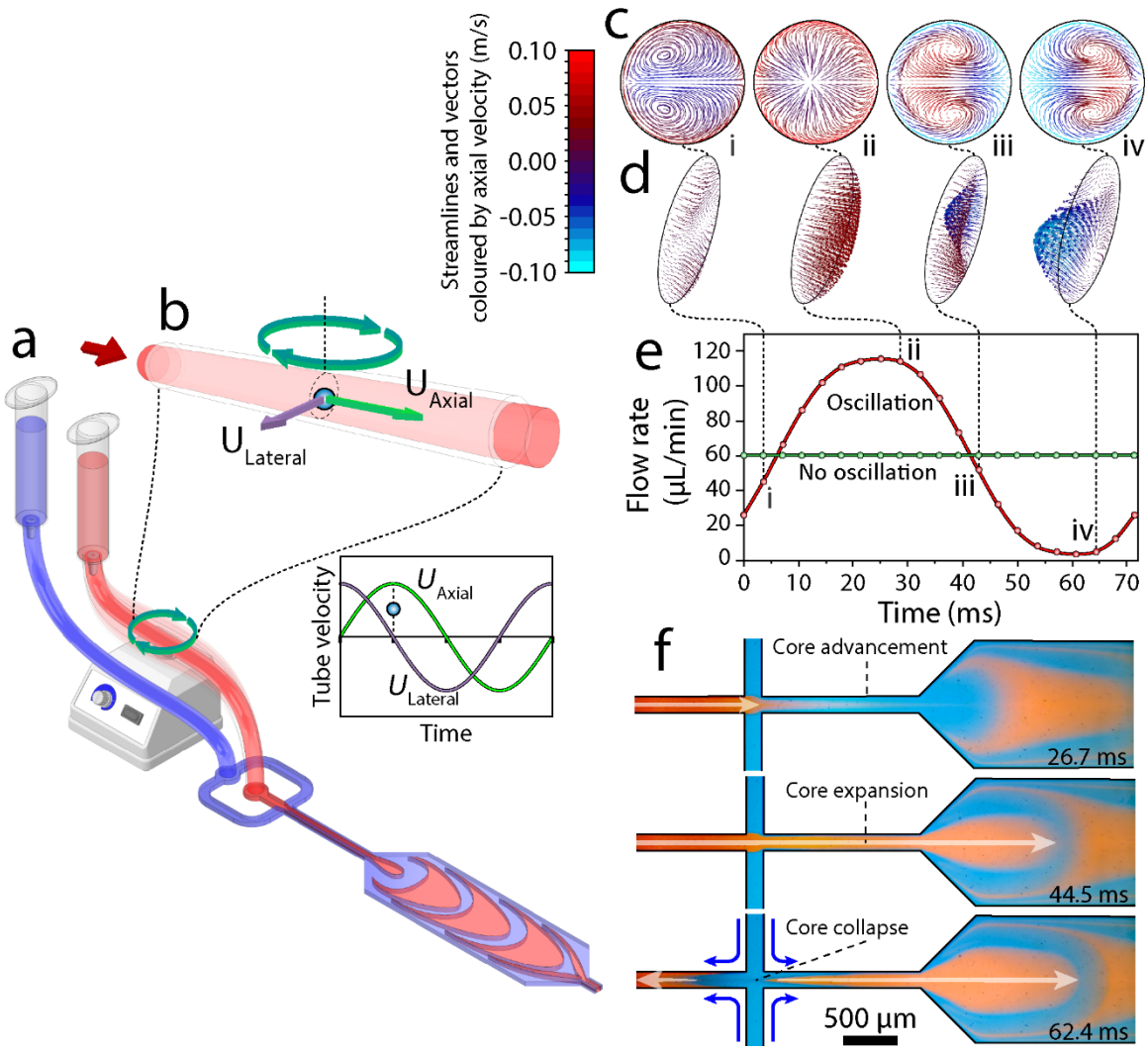

Figure 1. Oscillation of the core inlet tube leads to the generation of harmonic flow patterns in the microfluidic flow focusing system: **(a)** Schematics showing a microfluidic flow focusing system interfaced with core and sheath flow tubes in which the core inlet tube is oscillated using a commercially available vortexer, **(b)** Tube oscillation leads to induction of lateral and axial tube velocities, **(c-d)** Numerical simulations reveal the formation of harmonic vortices and velocity vectors in the oscillating tube, **(e)** This leads to harmonic variations of the core flow rate, **(f)** This results in the harmonic expansion and contraction of the core flow at the junction of the core and sheath flows.

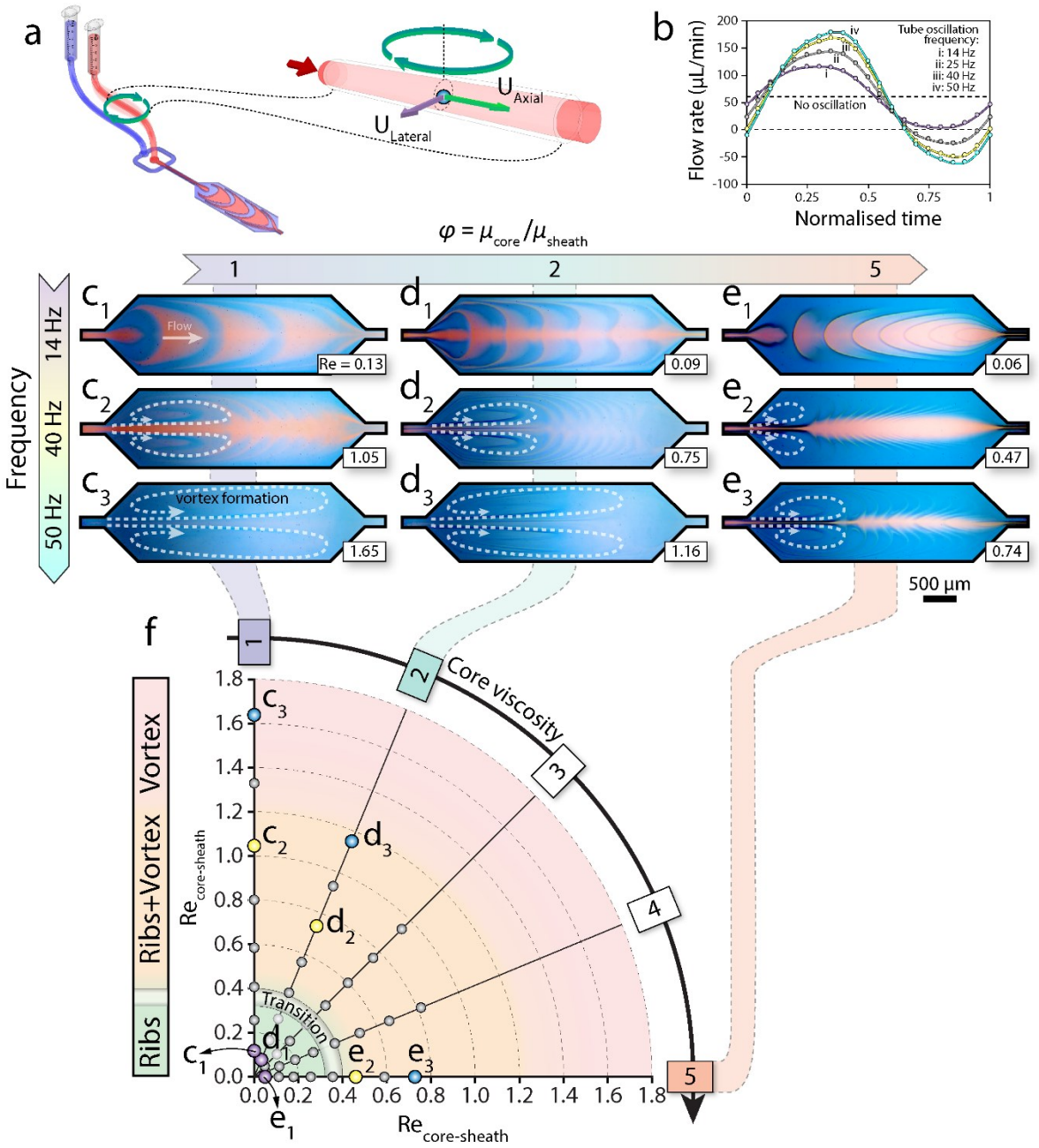

Figure 2. Generation of dynamic flow patterns inside the expansion chamber of a microfluidic system when setting the magnitude of tube oscillation to 2.5 mm: **(a)** Schematics showing the oscillation of the core tube, **(b)** Temporal variations of core flow rate when oscillating the core tube at frequencies ranging from 14 to 50 Hz, **(c-e)** Generation of harmonic rib and vortex patterns at various tube oscillation frequencies ranging from 14 to 50 Hz and core-to-sheath flow viscosity ratios ranging from 1 to 5, **(f)** Flow pattern map showing the transition from rib to vortex mode according to the Reynolds number of adjacent core and sheath flows, obtained from at least 150 independent experiments.

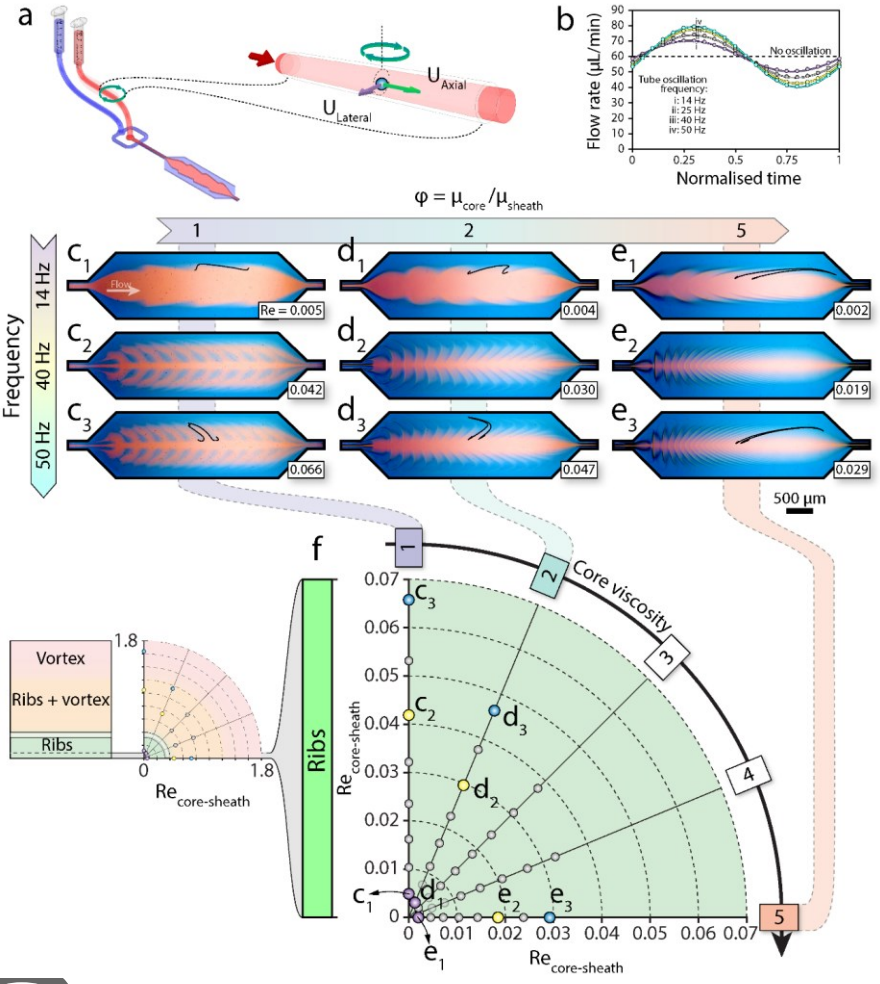

Figure 3. Generation of dynamic flow patterns inside the expansion chamber of a microfluidic system when reducing the magnitude of tube oscillation to 0.5 mm: **(a)** Schematics showing the oscillation of the core tube, **(b)** Temporal variations of core flow rate when oscillating the core tube at 14 and 50 Hz, **(c-e)** Generation of harmonic rib patterns at various tube oscillation frequencies ranging from 14 to 50 Hz and core-to-sheath flow viscosity ratios ranging from 1 to 5, **(f)** Flow

pattern map showing the dominance of 'rib' mode across the entire frequency range and viscosity ratios, obtained from at least 150 independent experiments.

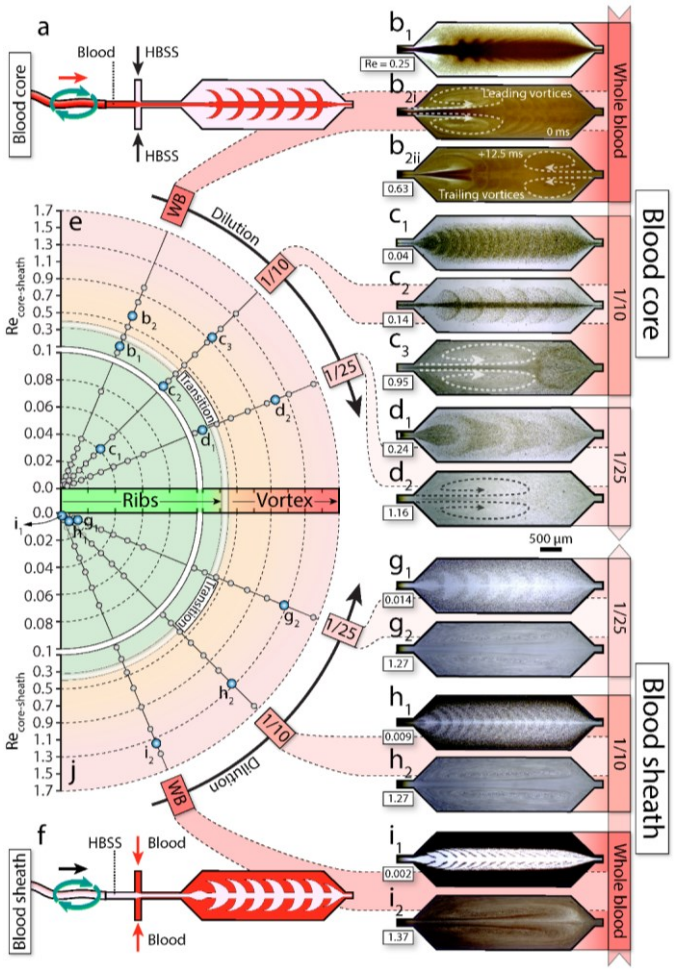

Figure 4. Generation of dynamic flow patterns using human blood samples: **(a)** Schematics showing the application of blood through the oscillating core tube, **(b-d)** Dynamic flow patterns obtained at various Reynolds numbers when applying whole or diluted blood through the oscillating core tube, **(e)** Flow pattern map showing the transition from rib to vortex mode when applying blood through the oscillating core tube, obtained from at least 200 independent experiments, **(f)** Schematics showing the application of blood through the sheath tube, **(g-i)** Dynamic flow patterns obtained at various Reynolds numbers when applying whole or diluted blood through the sheath tube, **(j)** Flow

pattern map when applying blood through the sheath inlet while applying HBSS through the oscillating core tube, obtained from at least 200 independent experiments.

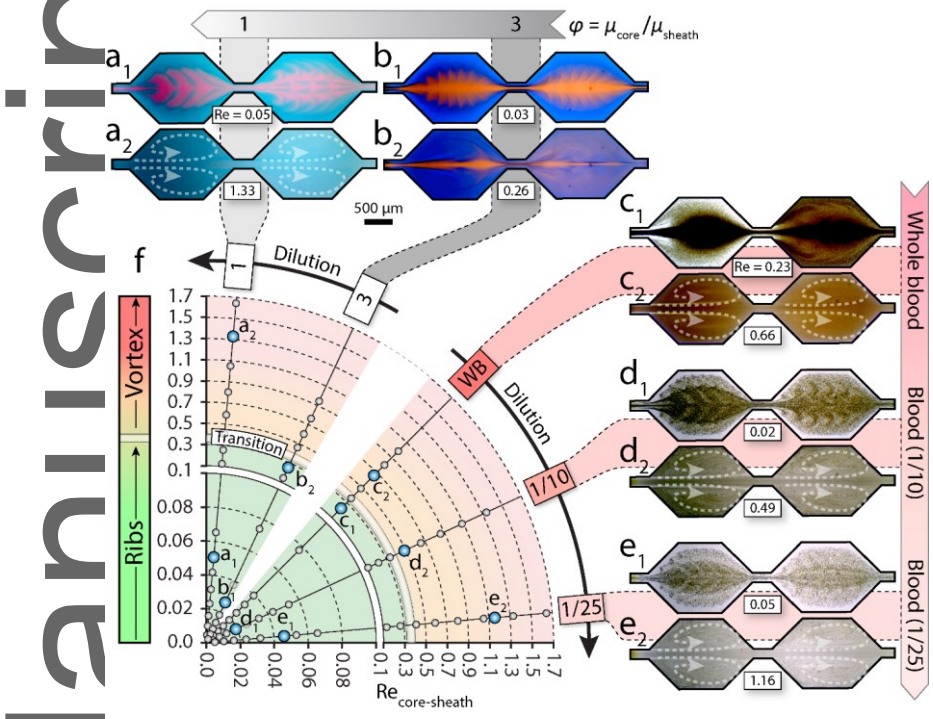

Figure 5. Formation of superimposed rib and vortex flow patterns using serial microfluidic chambers when oscillating the core inlet tube at 40 Hz: **(a-b)** Water-glycerol mixtures applied through the core inlet at different core to sheath viscosity ratios of 1 and 3, **(c-e)** Blood samples diluted with HBSS at different ratios of 1:0 (whole blood), 1:10 and 1:25 applied through the core inlet, **(f)** Flow pattern map showing the transition from rib to vortex mode, obtained from at least 150 independent experiments.

Table of content:

Oscillation of inlet tubes is demonstrated as an effective manner for generating harmonic flow patterns in microfluidic systems. Harmonic rib or vortical flow patterns can be generated in water-based solutions or blood samples, the dynamics of which can be modulated by the frequency and magnitude of tube oscillation.

microfluidics, inertial, dynamic flow patterns

P. Thurgood*, S. A. Suarez, E. Pirogova, A. R. Jex, K. Peter, S. Baratchi, K. Khoshmanesh*

Tunable harmonic flow patterns in microfluidic systems through simple tube oscillation